Qutrit quantum battery: Comparing different charging protocols

Giulia Gemme,[1,*] Michele Grossi,[2] Sofia Vallecorsa,[2] Maura Sassetti,[1,3] and Dario Ferraro[1,3]
[1]*Dipartimento di Fisica, Università di Genova, Via Dodecaneso 33, 16146 Genova, Italy*
[2]*CERN, 1 Esplanade des Particules, CH-1211 Geneva, Switzerland*
[3]*CNR-SPIN, Via Dodecaneso 33, 16146 Genova, Italy*

(Received 24 October 2023; revised 7 March 2024; accepted 22 March 2024; published 24 April 2024)

Motivated by recent experimental observations carried out in superconducting transmon circuits, we compare two different charging protocols for three-level quantum batteries based on time-dependent classical pulses. In the first case, the complete charging is achieved through the application of two sequential pulses, while in the second the charging occurs in a unique step applying the two pulses simultaneously. The latter approach is characterized by a shorter charging time, and consequently by a greater charging power. Moreover, both protocols are analytically solvable, leading to a complete control on the dynamics of the quantum system and opening unique perspectives in the manipulation of the so-called qutrits. To support this analysis, we have tested both protocols on IBM quantum devices based on superconducting circuits in the transmon regime. The minimum achieved charging time represents one of the fastest stable charging reported so far in solid-state quantum batteries.

DOI: 10.1103/PhysRevResearch.6.023091

I. INTRODUCTION

Quantum batteries (QBs) are miniaturized devices able to efficiently store and release energy on demand, exploiting the puzzling rules of quantum mechanics [1,2]. They are intended to play a major role in the future developments of quantum technologies [3,4]. In this direction, it is possible to imagine, for example, networks of QBs connected to a quantum computer with the aim of locally providing the energy supply to support reversible quantum operations [5–7]. The starting point of this field can be traced back to the seminal work by Alicki and Fannes in 2013 [8]. Since then, theoretical investigations have focused on the study of the charging dynamics of one or more quantum systems, each one with a finite dimension Hilbert space, usually two-level systems (TLSs) [9].

For what concerns the charging of QBs, two main approaches have been discussed in literature. The first one is based on the coherent energy transfer between a purely quantum charger and the QB [10–13]. This case has been discussed, in particular, for arrays of artificial atoms [14–19] and systems for cavity in circuit quantum electrodynamics [20–31]. Remarkably enough, experimental evidence of a quantum charged QB has been recently reported in a system where fluorescent organic molecules play the role of TLSs embedded in a microcavity [32]. This system shows a behavior consistent to that predicted in Ref. [20], with dissipative effects counterintuitively leading to an improvement of the stability of the QBs [23].

On the other hand, the charging induced by a classical external drive has also been considered [33–35]. This idea culminated in the first experimental evidence of a three-level QB realized with a superconducting circuit in the transmon regime [36]. The authors of this work compared different charging protocols able to promote a qutrit (three-level quantum system) from the ground state to a second excited state. In particular, they reasonably assume that the maximum admissible amplitude for the independently applied drives is bounded both at the level of the intensity or in modulus. Exactly saturating these bounds, they have been able to apply the quantum brachistochrone theory [37] to obtain analytically solvable stable adiabatic charging protocols. By controlling the sequence of these applied drives, they have been able to obtain both fast and unstable and slow and stable charging processes. This latter case shows charging times of the order of $\approx$200 ns, namely, two orders of magnitude shorter with respect to the typical relaxation and dephasing times of the considered device ($\approx$20 μs).

In the present paper, we will demonstrate that a full analytical description of the qutrit's dynamics is possible under more general conditions where the bound in the amplitude of the drives is fulfilled but not saturated. In this case, the possibility to exactly solve the dynamics of the system relies on the rotating wave approximation (RWA) and not on adiabatic considerations. Reviewing the recently discussed case of a qubit QB, we will identify faster stable protocols able to realize an almost complete charging of the qutrit QB. In particular, driving the systems with properly modulated Gaussian pulses, we will determine the charging time considering (i) a sequential charging protocol where the qutrit is first promoted from the ground to the first excited state and afterwards from the first

*giulia.gemme@edu.unige.it

to the second excited state and (ii) a simultaneous charging protocol where the transition directly involve the ground and the second excited state.

We will test these protocols on IBM quantum devices showing that in the simultaneous protocol, the charging time can be decreased down to ≈20 ns. This is an order of magnitude shorter with respect to that observed in Refs. [36,38] in the presence of a comparable stored energy and longer relaxation and dephasing times (≈100 μs). This is a consequence of the stronger intensity of the matter-radiation coupling in the considered devices. To the best of our knowledge, this represents the fastest stable charging reported so far in the framework of QBs based on superconducting circuits, indicating that IBM quantum devices are ideal candidates to develop stable multilevel solid-state QBs.

II. TWO-LEVEL QB

We start our analysis by reviewing the case of a superconducting circuit in the transmon regime working as a qubit (see Ref. [39] and Appendix A for more details). To access quantum features, these devices are put at cryogenic temperatures (few mK). Under these working conditions, which are conventionally used in the framework of solid state quantum computation [40], the QB can be effectively described as a TLS with Hamiltonian (from now on, we consider $\hbar = 1$)

$$\hat{H}^{(2)}_{\rm QB} = \omega_0|0\rangle\langle 0| + \omega_1|1\rangle\langle 1| \tag{1}$$

and level spacing

$$\Delta = \omega_1 - \omega_0 \tag{2}$$

between the ground state $|0\rangle$ and the first excited state $|1\rangle$. Its dynamics is controlled by means of a classical external time-dependent drive such that the total Hamiltonian reads [41,42]

$$\hat{H}^{(2)}(t) = \hat{H}^{(2)}_{\rm QB} + \hat{H}^{(2)}_{C}(t), \tag{3}$$

with

$$\hat{H}^{(2)}_{C}(t) = g f(t)\cos(\Omega t)(|0\rangle\langle 1| + |1\rangle\langle 0|). \tag{4}$$

In the above equation, $f(t)$ is a time-dependent envelope function with maximum amplitude equal to one, whose form will be specified in the following. Such function is further modulated by a cosine with controllable frequency Ω. Finally, g represents the intensity of the (dipole) coupling between the QB and the classical drive. Notice that in our study we can safely neglect the dynamics of the external charger, due to the fact that it can be considered as a classical object not affected by the state of the QB [34].

To study the time evolution of the state and, consequently, the time behavior of the stored energy stored, we consider the generic initial wave function at time $t = 0$ [38],

$$|\psi(0)\rangle = \sqrt{a}|0\rangle + \sqrt{1-a}e^{i\phi}|1\rangle, \tag{5}$$

with $0 \leqslant a \leqslant 1$ and $0 \leqslant \phi < 2\pi$ real parameters. The experimentally realized transmon devices, typically used in the quantum computing framework, including the devices developed by IBM, usually satisfy $g \ll \Delta$ (with typically more then an order of magnitude between the two quantities) [40]. Under this condition, to achieve a complete charging of the QB, namely, a perfect transition $|0\rangle \to |1\rangle$, one needs to tune the frequency of the drive in such a way to precisely fulfill the condition $\Omega = \Delta$. At this point, it is useful to consider the time-dependent rotation

$$\hat{S}^{(2)}(t) = e^{i\hat{H}^{(2)}_{\rm QB}t}, \tag{6}$$

leading, in the rotating frame, to the new Hamiltonian

$$\hat{H}'^{(2)} = \hat{S}^{(2)}\hat{H}^{(2)}(\hat{S}^{(2)})^{\dagger} - i\hat{S}^{(2)}\frac{d(\hat{S}^{(2)})^{\dagger}}{dt}. \tag{7}$$

Further considering the RWA [43–45], which is very well justified under the conditions of resonance and small coupling discussed above [46], as we have also checked numerically for experimentally relevant values of the parameters (not shown), one obtains the effective Hamiltonian

$$\hat{H}^{(2)}_{\rm eff}(t) = \frac{g}{2}f(t)(|0\rangle\langle 1| + |1\rangle\langle 0|), \tag{8}$$

where we have omitted a constant term that plays no role in the dynamics. This leads to the Schrödinger equation

$$i|\dot{\psi}'(t)\rangle = \hat{H}^{(2)}_{\rm eff}|\psi'(t)\rangle, \tag{9}$$

where $|\psi'(t)\rangle = \hat{S}^{(2)}(t)|\psi(t)\rangle$ with $|\psi(t)\rangle$ the wave function of the qubit at a given time [38]. Note that we are using the conventional Newton's dot notation to indicate the time derivative.

Starting from this, the energy stored in the QB at the same time t can be defined as [10,20]

$$E^{(2)}(t) = \langle\psi(t)|\hat{H}^{(2)}_{\rm QB}|\psi(t)\rangle. \tag{10}$$

According to this definition and taking into account the analysis described above, the energy stored into the QB at the time t can be explicitly written (assuming for now on ω_0 as the energy reference) as

$$E^{(2)}(t) = \Delta\Bigg[a\sin^2\frac{\theta(t)}{2} + (1-a)\cos^2\frac{\theta(t)}{2} \tag{11}$$

$$+ 2\sqrt{a}\sqrt{1-a}\sin\phi\sin\frac{\theta(t)}{2}\cos\frac{\theta(t)}{2}\Bigg], \tag{12}$$

where

$$\theta(t) = g\int_0^t f(\tau)d\tau. \tag{13}$$

According to this expression, the key parameter to control the system's dynamics is the area under the envelope function $f(t)$. However, to evaluate the energy stored in the QB as a function of time, the knowledge of the form of $f(t)$ is therefore necessary. According to the analysis reported in Ref. [38], a good choice for the envelope function is

$$f(t) = \mathcal{N}e^{-\frac{(t-t_m/2)^2}{2\sigma^2}}, \tag{14}$$

namely, a Gaussian with amplitude $\mathcal{N}$ and standard deviation σ, centered at $t = t_m/2$, with t_m the time at which the measurement of the state is carried out. In the following, we will assume

$$\sigma = \frac{t_m}{8}, \tag{15}$$

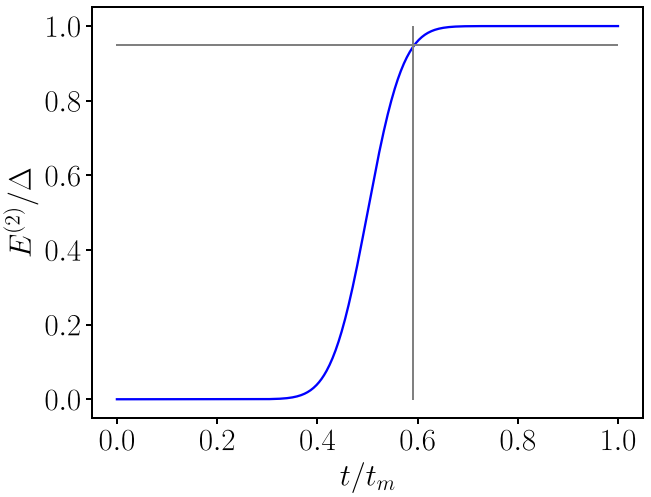

FIG. 1. Blue curve: Theoretical behavior of the energy $E^{(2)}$ stored into the qubit QB (in units of Δ) as a function of t (in units of t_m) and with initial condition $|\psi(t)\rangle = |0\rangle$ [$a = 1$ and arbitrary ϕ in (5)]. Horizontal grey line indicates a QB charging of $E^{(2)}_{\rm thr} = 0.95\Delta$, while the vertical grey line is in correspondence with the charging time $t_c = 0.59t_m$. Here we are considering $\theta_m = \pi$.

where the condition $t_m \gg \sigma$ is fulfilled, and

$$\mathcal{N} = \frac{\theta_m}{(g\sigma\sqrt{2\pi})}, \tag{16}$$

with θ_m the total phase induced by the application of the pulse.

Indeed, one has

$$\theta(t) \approx \frac{\theta_m}{2}\left[\mathrm{Erf}\left(\frac{t-\frac{t_m}{2}}{\sqrt{2}\sigma}\right)+1\right], \tag{17}$$

with $\mathrm{Erf}(x)$ the error function of argument x. This leads to $\theta \approx \theta_m$ for $t \approx t_m \gg \sigma$.

Replacing the above expression into (12), one can determine the charging time t_c, namely, the time at which the QB is (almost) completely charged, as a fraction of t_m. For example, in Fig. 1, the QB reaches a charging $E^{(2)}_{\rm thr} = 0.95\Delta$ for a time $t_c = 0.59t_m$.

It is also useful to consider more realistic situations. Indeed, according to the analysis reported in Ref. [38], in a real device it is not possible to initialize the system exactly in the ground state. According to this, considering, for example, the conditions $a = 0.98$, $\phi = 0$ [Fig. 2(a)], and $a = 0.96$, $\phi = 0$ [Fig. 2(b)], the charging $E^{(2)}_{\rm thr} = 0.95\Delta$ is achieved for $t_c = 0.61t_m$ and $t_c = 0.63t_m$, respectively.

Obviously, the arbitrary choice of the value for the threshold $E^{(2)}_{\rm thr}$ could, in general, play a relevant role in determining the charging time. However, assuming $E^{(2)}_{\rm thr}$ ranging from 0.92Δ to 0.99Δ, the charging times are only marginally different, namely, $t_c \approx 0.6t_m$ (see Table I). This strengthens the validity of our estimation.

Despite the above analysis, the charging behavior in real time cannot be directly addressed in a cloud-based access as the one provided by IBM. However, it is possible to reconstruct it starting from the evolution of the stored energy by fixing the time at $t = t_m \gg \sigma$ and by changing the amplitude

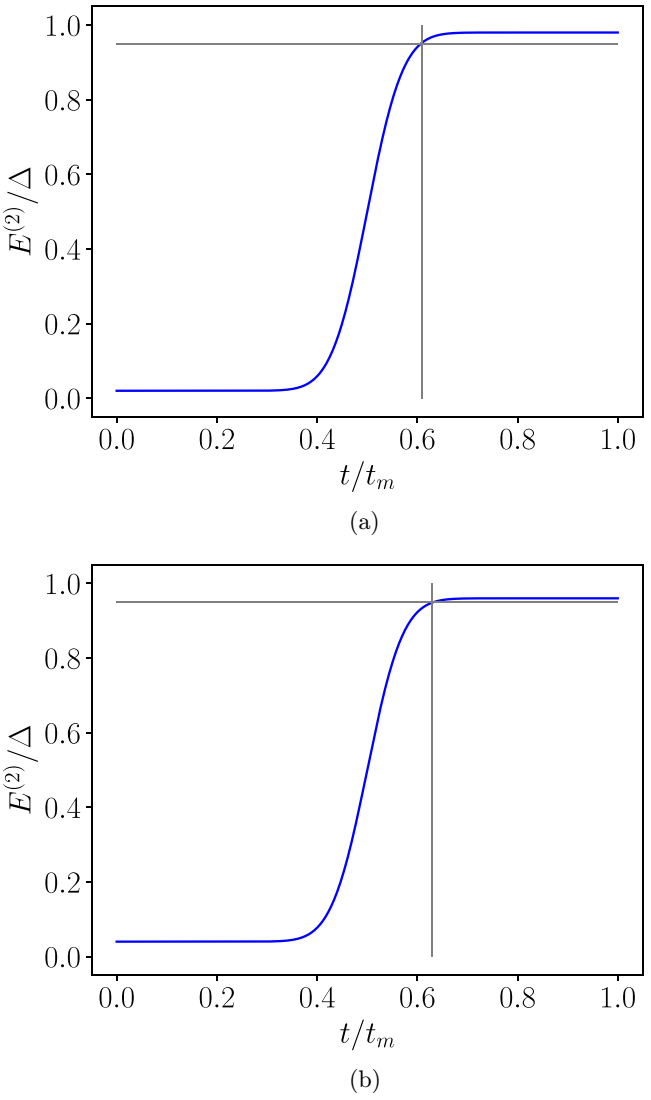

FIG. 2. Blue curves: Theoretical behavior of the energy $E^{(2)}$ stored into the qubit QB (in units of Δ) as a function of t (in units of t_m) and with $a = 0.98$, $\phi = 0$ (a) and $a = 0.96$, $\phi = 0$ (b), respectively. We have considered $E^{(2)}_{\rm thr} = 0.95\Delta$ in both panels (horizontal grey lines). This leads to $t_c = 0.61t_m$ (a) and $t_c = 0.63t_m$ (b), respectively (vertical grey lines). Here we are considering $\theta_m = \pi$.

TABLE I. Charging times (in units of t_m) for different initial states of the QB [denoted by a and ϕ according to (5)] and values of the energy threshold.

a	ϕ	$E_{\rm thr}/\Delta$	t_c/t_m
1	0	0.92	0.58
1	0	0.95	0.59
1	0	0.99	0.63
0.98	0	0.95	0.61
0.98	$\frac{\pi}{4}$	0.95	0.63
0.96	0	0.95	0.63
0.96	$\frac{\pi}{4}$	0.95	0.68

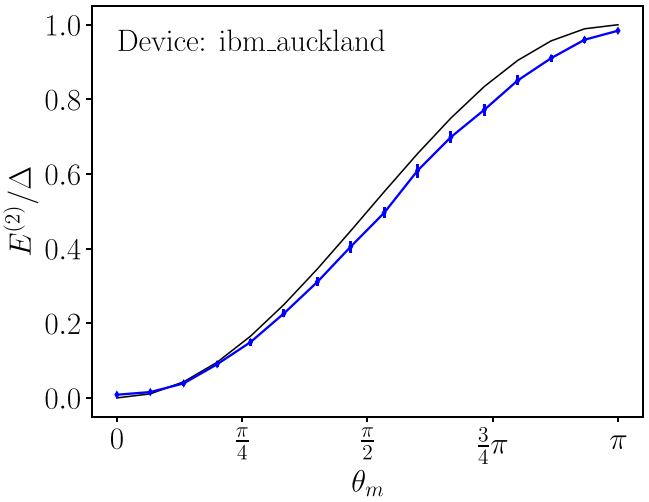

FIG. 3. Energy stored in the QB (in units of Δ) as a function of θ_m. The black line is obtained analytically using (18) and with initial condition $|\psi(t)\rangle = |0\rangle$ [$a = 1$ and arbitrary ϕ in (5)]. The blue points correspond to experimental data obtained from the *ibm_auckland* device, using the Gaussian pulses described in the main text with $t_m = 30$ ns.

of the applied pulse θ_m. According to this, one has

$$E^{(2)}(\theta(t = t_m)) \approx E^{(2)}(\theta_m) = a \sin^2 \frac{\theta_m}{2} + (1 - a) \cos^2 \frac{\theta_m}{2} + 2\sqrt{a}\sqrt{1 - a} \sin\phi \sin \frac{\theta_m}{2} \cos \frac{\theta_m}{2}. \quad (18)$$

The theoretical prediction for this quantity in the case of an ideal charging starting from the ground state $|0\rangle$ is reported in Fig. 3 and compared to the real data extracted from the IBM quantum machine *ibm_auckland*. Data are extracted from the machine following the calibration procedure described in Ref. [38]. Notice that this curve does not depend on the functional form of the drive, provided that $t_m \gg \sigma$ with σ the typical width associated to $f(t)$, and that the deviation with respect to the theoretical prediction mainly depends on the fact that the system cannot be initialized exactly in the ground state, that the pulses are discretized, and to possible readout errors [38]. Taking into account the fact that for this specific experiment, $t_m = 30$ ns and due to the above considerations, one can estimate a charging time $t_c \approx 20$ ns. This value is orders of magnitude shorter with respect to the decay time of the device ($\approx$100 μs), leading to a great stability of the QB [47]. Moreover, this time is shorter with respect to the one achieved in Ref. [38] due to the greater values of coupling characterizing *ibm_auckland* in comparison with the one of *ibm_armonk* used there ($g \approx 1$ GHz vs $g \approx 0.1$ GHz).

III. THREE-LEVEL QB

We want now to investigate the possibility of realizing charging protocols addressing the ground ($|0\rangle$) and first two excited states ($|1\rangle$, $|2\rangle$) of a transmon, namely, realizing a qutrit QB described by the Hamiltonian (see Appendix A for more details)

$$\hat{H}^{(3)}_{\rm QB} = \omega_0 |0\rangle\langle 0| + \omega_1 |1\rangle\langle 1| + \omega_2 |2\rangle\langle 2|. \quad (19)$$

Also in this case, the dynamics is controlled by means of classical external drives such that

$$\hat{H}^{(3)}(t) = \hat{H}^{(3)}_{\rm QB} + \hat{H}^{(3)}_C(t), \quad (20)$$

with

$$\hat{H}^{(3)}_C(t) = g f_1(t) \cos(\Omega_1 t)(|0\rangle\langle 1| + |1\rangle\langle 0|) + g f_2(t) \cos(\Omega_2 t)(|1\rangle\langle 2| + |2\rangle\langle 1|). \quad (21)$$

Here, $f_1(t)$ and $f_2(t)$ are two generally different time-dependent envelope functions generalizing that shown in the previous section.

Notice that the general form of the classical driving Hamiltonian in (21) allows for a direct coupling only between states with opposite parity ($|0\rangle \leftrightarrow |1\rangle$, $|1\rangle \leftrightarrow |2\rangle$). Despite the fact that a transition $|0\rangle \leftrightarrow |2\rangle$ could be useful for the following analysis, it cannot be implemented in these machines. The Hamiltonian in (21) has also been investigated in Ref. [36], assuming an adiabatic evolution where the functions $f_1(t)$ and $f_2(t)$ were properly constrained at the level of the maximum admissible amplitude. However, in the following we will discuss more versatile and efficient charging protocols, leading to a faster and more stable charging.

Proceeding in full analogy with what done in the case of the qubit QB, one can consider a time-dependent rotation of the form

$$\hat{S}^{(3)}(t) = e^{i\hat{H}^{(3)}_{\rm QB} t} \quad (22)$$

to describe the system in the rotating frame. To simplify the notation, one can define

$$\Delta = \omega_1 - \omega_0, \quad (23)$$

$$\Delta' = \omega_2 - \omega_1. \quad (24)$$

In the transmon geometry considered in this paper, one has $\Delta > \Delta'$ due to the fact that this device can be described as a anharmonic oscillator of the Duffing type (see Refs. [39,40] and Appendix A for more details). In this direction, the rotation introduced in Eq. (22) has the important advantage of getting rid of the $\hat{H}^{(3)}_{\rm QB}$ contribution of the Hamiltonian, allowing us to describe both an evenly spaced and a more realistic anharmonic case on the same ground. Moreover, it is worth noting that, also in this case, the condition $g \ll \Delta, \Delta'$ is typically well fulfilled.

Considering again the RWA, valid for $\Omega_1 = \Delta$ and $\Omega_2 = \Delta'$, the effective Hamiltonian in the rotating frame can be evaluate by means of the relation

$$\hat{H}'^{(3)}(t) = \hat{S}^{(3)} \hat{H}^{(3)} (\hat{S}^{(3)})^\dagger - i\hat{S}^{(3)} \frac{d(\hat{S}^{(3)})^\dagger}{dt} \quad (25)$$

and reads

$$\hat{H}^{(3)}_{\rm eff} = \frac{g}{2} f_1(t)(|0\rangle\langle 1| + |1\rangle\langle 0|) \quad (26)$$

$$+ \frac{g}{2} f_2(t)(|1\rangle\langle 2| + |2\rangle\langle 1|). \quad (27)$$

This leads to the Schrödinger equation

$$i|\dot{\Psi}'(t)\rangle = \hat{H}^{(3)}_{\rm eff} |\Psi'(t)\rangle, \quad (28)$$

where $|\Psi'(t)\rangle = \hat{S}^{(3)}(t)|\Psi(t)\rangle$, with $|\Psi(t)\rangle$ the wave function of the qutrit at a given time.

Considering the conventional spinorial notation

$$|\Psi'(t)\rangle = \begin{pmatrix} c_2(t) \\ c_1(t) \\ c_0(t) \end{pmatrix}, \tag{29}$$

the dynamics of the system is obtained by solving the set of differential equations

$$\begin{pmatrix} \dot{c}_2(t) \\ \dot{c}_1(t) \\ \dot{c}_0(t) \end{pmatrix} = -i\frac{g}{2}\begin{pmatrix} 0 & f_2(t) & 0 \\ f_2(t) & 0 & f_1(t) \\ 0 & f_1(t) & 0 \end{pmatrix}\begin{pmatrix} c_2(t) \\ c_1(t) \\ c_0(t) \end{pmatrix}. \tag{30}$$

According to the previous discussion, to excite the QB from $|0\rangle$ to $|2\rangle$ we have to apply two pulses to the system. To achieve this goal, in the two following subsections we will address two different situations: (i) the two pulses are applied sequentially and (ii) two pulses are simultaneous. As will be clear in the following, both cases can be treated analytically. From a theoretical point of view, intermediate situations where the two pulses partially overlap can also be studied by considering a numerical approach, however, we are not going to discuss these cases in detail because it not easy to directly implement them on IBM machines [48]. It is worth noting that, besides the application in the framework of QBs, a deeper understanding of the dynamics of a qutrit is relevant to characterize the behavior of quantum devices outside the conventional schemes of quantum computation [49].

In the following, we will evaluate the energy stored in the three-level QB,

$$E^{(3)}(t) = \langle\Psi(t)|\hat{H}^{(3)}_{\rm QB}|\Psi(t)\rangle, \tag{31}$$

assuming the ground state of the qutrit as initial state, namely,

$$|\Psi(0)\rangle = |0\rangle. \tag{32}$$

We will also comment about possible deviations with respect to this ideal condition in realistic implementations. Note that, despite the different physical implementation and objectives, the formalism we are considering presents analogies with recently reported protocols for coherent energy transfer [50].

A. Sequential charging protocol

Here, we can choose two identical, but properly delayed in time, pulses, namely, $f_2(t) = f_1(t - t_m/2)$ and with $f_1(t)$ of the same Gaussian form as in (14) but with $t_m \to t_m/2$, in such a way that the total duration of the protocol is t_m. In this limit, one can analytically solve the problem in two steps, each one identical to that previously discussed in the case of the qubit.

1. $|0\rangle \to |1\rangle$ *transition*

In this case, one needs to solve the set of differential equations:

$$\begin{pmatrix} \dot{c}_2(t) \\ \dot{c}_1(t) \\ \dot{c}_0(t) \end{pmatrix} = -i\frac{g}{2}\begin{pmatrix} 0 & 0 & 0 \\ 0 & 0 & f_1(t) \\ 0 & f_1(t) & 0 \end{pmatrix}\begin{pmatrix} c_2(t) \\ c_1(t) \\ c_0(t) \end{pmatrix}. \tag{33}$$

The energy stored in the QB in this phase is [see (12) with $a = 1$]

$$E^{(3)}_{\rm seq}(t) = \Delta \sin^2 \frac{\theta_1(t)}{2}, \tag{34}$$

with

$$\theta_1(t) = g\int_0^t f_1(\tau)d\tau \tag{35}$$

and $t \in [0, t_m/2]$. Note that one can safely assume that out of this interval, $f_1(t)$ is essentially zero.

2. $|1\rangle \to |2\rangle$ *transition*

Here, we need to solve the set of differential equations:

$$\begin{pmatrix} \dot{c}_2(t) \\ \dot{c}_1(t) \\ \dot{c}_0(t) \end{pmatrix} = -i\frac{g}{2}\begin{pmatrix} 0 & f_2(t) & 0 \\ f_2(t) & 0 & 0 \\ 0 & 0 & 0 \end{pmatrix}\begin{pmatrix} c_2(t) \\ c_1(t) \\ c_0(t) \end{pmatrix}. \tag{36}$$

Assuming that in the previous step the system reaches the first excited state ($|\Psi(t_m/2)\rangle \approx |1\rangle$), the energy stored in the QB is given by

$$E^{(3)}_{\rm seq}(t) = \Delta + \Delta' \sin^2 \frac{\theta_2(t)}{2}, \tag{37}$$

with

$$\theta_2(t) = g\int_{\frac{t_m}{2}}^t f_2(\tau)d\tau \tag{38}$$

and $t \in [t_m/2, t_m]$. Also in this case, out of this interval, $f_2(t)$ can be considered as null. Using the same Gaussian envelope function discussed in the previous section, with $\sigma = t_m/16$, one has

$$\theta_1(t) \approx \frac{\theta_{1,m}}{2}\left[\mathrm{Erf}\left(\frac{t - \frac{t_m}{4}}{\sqrt{2}\sigma}\right) + 1\right], \tag{39}$$

$$\theta_2(t) \approx \frac{\theta_{2,m}}{2}\left[\mathrm{Erf}\left(\frac{t - \frac{3t_m}{4}}{\sqrt{2}\sigma}\right) + 1\right]. \tag{40}$$

In Fig. 4, we show the energy stored in the battery as a function of time. Here, one can clearly see a two-step charging (blue curve). For what concerns the charging time, due to the similarity with the qubit charging, the same estimation discussed above also works here, limited to the second step ($t_c \approx 0.8t_m$).

Also in this case, the real time-dynamics cannot be accessed directly in IBM quantum devices. It is, however, possible to proceed in analogy with that done for the qubit, extracting it from the behavior of the energy stored at the final measurement time $t = t_m$ and changing the pulse amplitude, which can be redefined as

$$\varphi_m = \begin{cases} \theta_{1,m} & \text{if } \theta_{1,m} \in [0, \pi] \\ \pi + \theta_{2,m} & \text{if } \theta_{1,m} = \pi \,\&\, \theta_{2,m} \in [0, \pi]. \end{cases} \tag{41}$$

This definition has been introduced to keep track of the fact that as long as the total amplitude is smaller then π, we are considering $|0\rangle \to |1\rangle$, while for a total amplitude greater then π we are addressing the $|1\rangle \to |2\rangle$ transition.

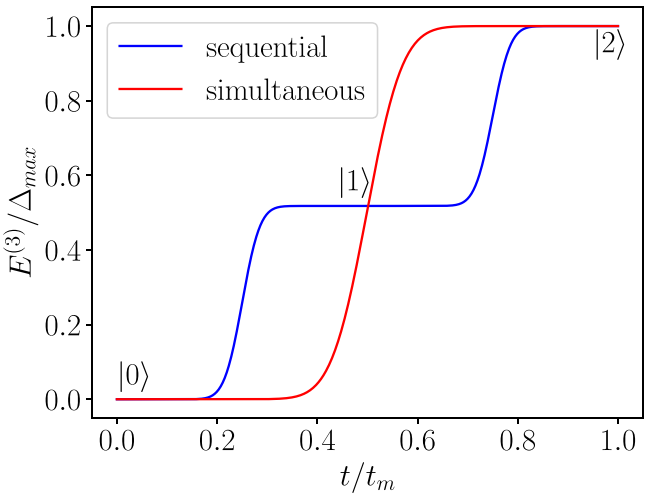

FIG. 4. Energy stored in the QB (in units of $\Delta_{\max} = \Delta + \Delta'$) as a function of t (in units of t_m) for both a sequential (blue curve) and simultaneous (red curve) charging protocol. Here we have considered pulses of Gaussian form, satisfying the constrains discussed in the main text, with $\varphi_m = 2\pi$, $\Theta_m = \pi$, and $a = 1$.

In terms of this new variable, one has

$$E^{(3)}_{\text{seq}}(\varphi_m) = \begin{cases} \Delta \sin^2 \frac{\varphi_m}{2} & \text{if } \varphi_m \in [0, \pi] \\ \Delta + \Delta' \sin^2 \left(\frac{\varphi_m - \pi}{2}\right) & \text{if } \varphi_m \in [\pi, 2\pi]. \end{cases} \tag{42}$$

The behavior of the above function, together with the relative experimental data obtained using the *ibm_auckland* device (a machine composed by 27 transmon circuits, of which we address the number 0 that is characterized by the the best compromise between the longer relaxation and dephasing times and the smaller readout error), are reported in Fig. 5 [51]. Data are extracted from the machine following the calibration procedure described in Appendix B. The

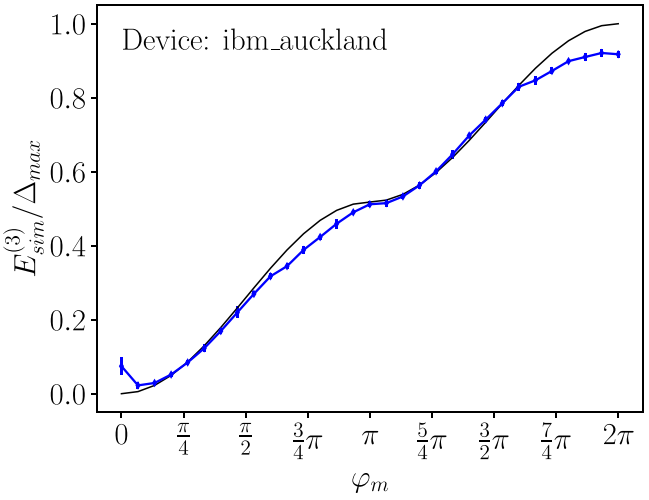

FIG. 5. Energy stored in the QB (in units of $\Delta_{\max}$) as a function of φ_m following the sequential charging protocol. The black line is obtained analytically using (42). The blue points correspond to experimental data obtained from the *ibm_auckland* device, using the Gaussian pulses described in the main text with $t_m = 30$ ns.

agreement between data and the theoretical function is very good, in particular, in the first half of each step. However, the experimental data show that it is not possible to fully charge the QB. Indeed, the maximum energy reached is 92.1% of the maximum energy $\Delta_{\max} = \Delta + \Delta'$.

Here, the charging occurs in a time ($t_c \approx 25$ ns), which is way shorter with respect to the decay time of the device ($\approx$100 μs). This stable charging protocol is similar to the one discussed in Ref. [36], although there the charging was reached in the longer time $t_c \approx 200$ ns. This faster charging is a consequence of the stronger dipole coupling characterizing this quantum device. For what concerns the amount of energy stored in the qutrit, one has $\Delta_{\max} \approx 39.2$ μeV, which is smaller but of the same order of magnitude of the one reported in Ref. [36] ($\Delta_{\max} \approx 50.6$ μeV).

B. Simultaneous charging protocol

In this case, one has $f_1(t) = f_2(t) = f(t)$, which leads to the set of differential equations:

$$\begin{pmatrix} \dot{c}_2(t) \\ \dot{c}_1(t) \\ \dot{c}_0(t) \end{pmatrix} = -i\frac{g}{2} f(t) \begin{pmatrix} 0 & 1 & 0 \\ 1 & 0 & 1 \\ 0 & 1 & 0 \end{pmatrix} \begin{pmatrix} c_2(t) \\ c_1(t) \\ c_0(t) \end{pmatrix}. \tag{43}$$

We underlie the fact that the particularly simple form of the above Schöedinger equation is a direct consequence of working in the rotating frame and in the RWA with a careful fine tuning of the drive frequencies with the level spacings of the qutrit. The matrix

$$\hat{T} = \begin{pmatrix} 0 & 1 & 0 \\ 1 & 0 & 1 \\ 0 & 1 & 0 \end{pmatrix} \tag{44}$$

is diagonalized by means of the unitary transformation

$$\hat{\mathcal{U}} = \begin{pmatrix} \frac{1}{2} & -\frac{1}{\sqrt{2}} & \frac{1}{2} \\ \frac{1}{2} & \frac{1}{\sqrt{2}} & \frac{1}{2} \\ \frac{1}{\sqrt{2}} & 0 & \frac{1}{\sqrt{2}} \end{pmatrix}. \tag{45}$$

This leads to a new set of the decoupled equations:

$$\begin{pmatrix} \dot{c}_-(t) \\ \dot{c}_+(t) \\ \dot{c}_B(t) \end{pmatrix} = -i\frac{g}{2} f(t) \begin{pmatrix} -\sqrt{2}c_-(t) \\ \sqrt{2}c_+(t) \\ 0 \end{pmatrix} \tag{46}$$

$$\rightarrow \quad \begin{cases} c_-(t) = e^{i\frac{g}{\sqrt{2}}\int_0^t f(\tau)d\tau} c_-(0) \\ c_+(t) = e^{-i\frac{g}{\sqrt{2}}\int_0^t f(\tau)d\tau} c_+(0) \\ c_B(t) = c_B(0). \end{cases} \tag{47}$$

In this basis, the state at time t is given by

$$|\Psi'(t)\rangle = \begin{pmatrix} e^{i\Theta(t)} c_-(0) \\ e^{-i\Theta(t)} c_+(0) \\ c_B(0) \end{pmatrix}, \tag{48}$$

with

$$\Theta(t) = \frac{g}{\sqrt{2}} \int_0^t f(\tau)d\tau. \tag{49}$$

Is this new basis, the initial conditions lead to

$$\begin{pmatrix} c_-(0) \\ c_+(0) \\ c_B(0) \end{pmatrix} = \begin{pmatrix} \frac{1}{2} \\ \frac{1}{2} \\ \frac{1}{\sqrt{2}} \end{pmatrix} \tag{50}$$

and, consequently,

$$|\Psi'(t)\rangle = \begin{pmatrix} \frac{1}{2}e^{i\Theta(t)} \\ \frac{1}{2}e^{-i\Theta(t)} \\ \frac{1}{\sqrt{2}} \end{pmatrix}. \tag{51}$$

Returning back to the original basis, we finally have

$$|\Psi'(t)\rangle = \begin{pmatrix} \frac{1}{2}[\cos\Theta(t) - 1] \\ -\frac{i}{\sqrt{2}}\sin\Theta(t) \\ \frac{1}{2}[\cos\Theta(t) + 1] \end{pmatrix}. \tag{52}$$

Considering the same Gaussian pulse as in the qubit case, one obtains

$$\Theta(t) = \frac{\Theta_m}{2}\left[\mathrm{Erf}\left(\frac{t - \frac{t_m}{2}}{\sqrt{2}\sigma}\right) + 1\right], \tag{53}$$

with $\Theta_m = \theta_m/\sqrt{2}$.

In Fig. 4, we report the energy stored in the QB as a function of time (red curve), given (assuming again ω_0 as the reference energy) by

$$E^{(3)}_{\mathrm{sim}}(t) = \frac{\Delta}{2}\sin^2\Theta(t) + \frac{\Delta_{\max}}{4}[1 - \cos\Theta(t)]^2. \tag{54}$$

As expected, the complete charging of the QB can be obtained here in a unique step as long as $\Theta_m = \pi$. Note that a similar form of the stored energy can be obtained under proper conditions within the adiabatic approximation (see Appendix C for more details).

Assuming, in analogy with that done for the qubit QB, the charging time as the one required to reach $E^{(3)}_{\mathrm{thr}} = 0.95\Delta_{\max}$, one has also in this case $t_c = 0.59t_m$. Note that, for a fix t_m, this leads to a faster charging (greater charging power) with respect to the sequential case.

In analogy to that done in the qubit case, the relative experimental data are reported, for $t_m \gg \sigma$, as a function of Θ_m:

$$E^{(3)}_{\mathrm{sim}}(\Theta_m) = \frac{\Delta}{2}\sin^2\Theta_m + \frac{\Delta_{\max}}{4}[1 - \cos\Theta_m]^2. \tag{55}$$

Data have been obtained using the *ibmq_toronto* device (a machine composed of 27 transmon circuits, of which we address the number 16 that is characterized by the best compromise between the longer relaxation and dephasing times and the smaller readout error) are reported in Fig. 6 [52]. It is worth noting that this simultaneous charging protocol cannot be implemented on all IBM quantum machines that can be accessed via qiskit-pulse due to software constraints [53]. Also in this case, data are obtained following the calibration procedure described in Appendix B. The maximum energy reached is 92.0% of $\Delta_{\max}$. This indicates that efficiencies of the two considered protocols are very close. Moreover, the charging occurs in roughly the same amount of time with respect to the other ($t_c \approx$ 20 ns) with an analogous relaxation

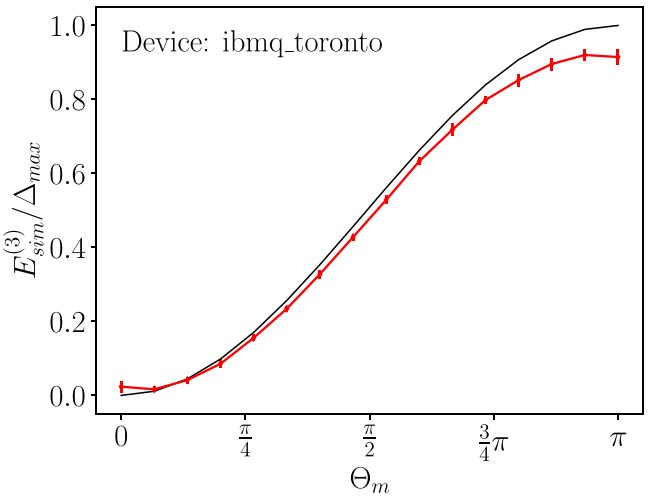

FIG. 6. Energy stored in the QB (in units of Δ_{max}) as a function of Θ_m following the simultaneous charging protocol. The black line is obtained analytically from Eq. (55). The red points correspond to experimental data, obtained from the *ibmq_toronto* machine. We have considered the same Gaussian pulse as in the qubit case with $t_m = 30$ ns.

time ($t_c \approx 100$ μs). As far as we know, this is the fastest stable charging process reported so far for a multilevel QB. Shorter times seem out of reach in the currently available IBM quantum devices due to discretization of the signal implemented at the level of software [38]. The amount of energy stored in the qutrit in this case is almost identical to the one reported for *ibm_auckland* ($\Delta_{\max} \approx 39.3$ μeV). It is worth mentioning the fact that the departure from the theoretical curve could be related to errors at the level of the initialization, due to discretization of pulses or to readout errors.

IV. CONCLUSIONS

We have considered two experimentally relevant cases in which the dynamics of a three-level QB can be treated analytically without any assumption, except the rotating wave approximation which is well justified in the considered range of parameters. Taking inspiration from an analysis carried out for the simpler two-level case, we have determined the charging time for (i) a sequential charging protocol where the qutrit is charged according to the two subsequent steps $|0\rangle \to |1\rangle$ and $|1\rangle \to |2\rangle$ and (ii) a simultaneous charging protocol where it is possible to achieve a direct $|0\rangle \to |2\rangle$ transition. We underline the fact that the reported results for both charging protocols are robust against crosstalk among the various circuits composing the considered machines.

We have also tested these protocols on IBM quantum devices estimating a charging time $t_c \approx 20 \div 25$ ns. These times are an order of magnitude shorter with respect to a previous analysis carried out in Ref. [36] and have been obtained for devices in with a comparable stored energy and characterized by longer relaxation and dephasing times. As far as we know, these results, in particular, for what it concerns the simultaneous charging, represent the fastest stable charging reported so far in the framework of multilevel solid state quantum batteries based on superconducting circuits.

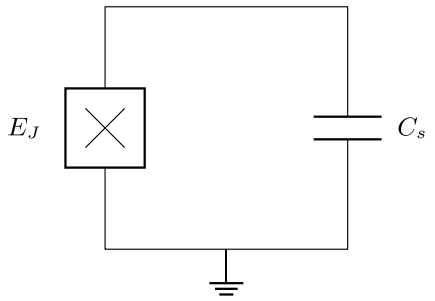

FIG. 7. Scheme of a superconducting circuit composed by a Josephson junction (crossed square symbols) with energy E_J and a capacitance C_s.

As an interesting byproduct of our analysis, we have shed light on the time-dependent control of multilevel quantum systems with relevant impact in the field of quantum computation. Indeed, the possibility to use quantum devices both as qubit and as qutrit [49] or, more generally, qudit [54] could make the current quantum computers more versatile, broadening the panorama of future possible applications [55].

ACKNOWLEDGMENTS

We thank G. M. Andolina, G. Benenti, N. Bronn, F. Campaioli, N. Earnest-Noble, and J. Quach for useful discussions. D.F. acknowledges the contribution of the European Union NextGenerationEU through the Quantum Busses for Coherent Energy Transfer (QUBERT) project, in the framework of the Curiosity Driven 2021 initiative of the University of Genova and through the Solid State Quantum Batteries: Characterization and Optimization (SoS-QuBa) project (Prot. No. 2022XK5CPX), in the framework of the PRIN 2022 initiative of the Italian Ministry of University (MUR) for the National Research Program (PNR). M.G. and S.V. are supported by CERN through CERN Quantum Technology Initiative. Access to IBM devices has been granted via CERN HUB. The views expressed are those of the authors and do not reflect the official policy or position of IBM or the IBM Quantum team.

APPENDIX A: THEORETICAL DESCRIPTION OF THE TRANSMON QUBIT

Here we want to provide a simple circuital scheme leading to the two- and three-level quantum devices discussed in the main text (see Fig. 7).

Its Hamiltonian is given by [39,40]

$$H = 4E_C N^2 - \frac{E_J}{2}\cos\Phi, \tag{A1}$$

with

$$E_C = \frac{e^2}{C_s} > 0 \tag{A2}$$

the charging energy associated to the capacitive part of the circuit (e here is the charging energy and C_s the capacitance), $E_J > 0$ the energy associated to the Josephson junction, N the Cooper pair number operator, and Φ the conjugate phase

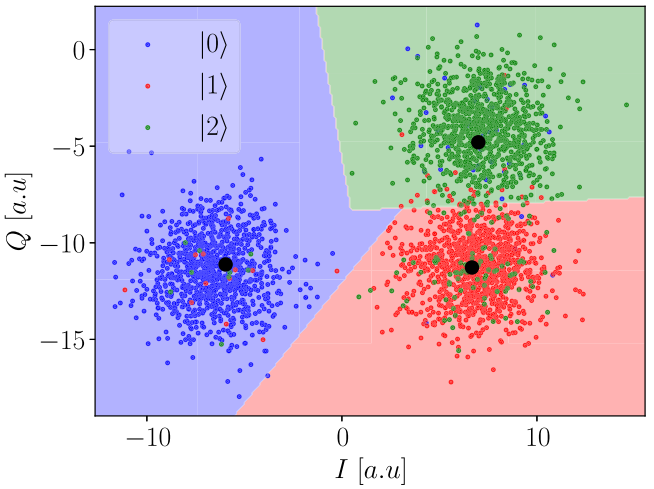

FIG. 8. Example of data distribution associated to the measurements of the state $|0\rangle$ (blue dots), $|1\rangle$ (red dots) and $|2\rangle$ (green dots) in the (I, Q) plane (in arbitrary units) for the *ibm_auckland* device. Big black dots indicate the centers of the different distributions, while straight lines separate the regions associated to every state. The efficiency of the considered separation is roughly 95.5% for the ground state, 95.7% for the first excited state, and 90.0% for the second excited state. For each state shown in the plot, we have considered 1024 runs (3072 in total).

operator. They satisfy the commutation relation

$$[\Phi, N] = i. \tag{A3}$$

In the transmon limit $E_C \ll E_J$, this problem maps into the one of a particle with very small kinetic energy trapped in a cosinelike potential. Under these conditions, it is possible to Taylor expand the cosine term up to fourth order, obtaining

$$H \approx 4E_C N^2 + \frac{E_J}{2}\Phi^2 - \frac{E_J}{24}\Phi^4. \tag{A4}$$

The previous Hamiltonian can be quantized introducing ladder operators satisfying

$$[b, b^\dagger] = 1 \tag{A5}$$

and such that

$$N = i\left(\frac{E_J}{32E_C}\right)^{\frac{1}{4}}(b^\dagger - b), \tag{A6}$$

$$\Phi = \left(\frac{2E_C}{E_J}\right)^{\frac{1}{4}}(b^\dagger + b). \tag{A7}$$

According to this, one obtains an anharmonic oscillator of the Duffing type,

$$H \approx \omega_P b^\dagger b - \frac{E_C}{12}(b^\dagger + b)^4, \tag{A8}$$

with

$$\omega_P = \sqrt{8E_C E_J} \tag{A9}$$

the so-called plasma frequency of the circuit.

In the considered limit, the energy levels are very well determined already at first order in perturbation theory, leading

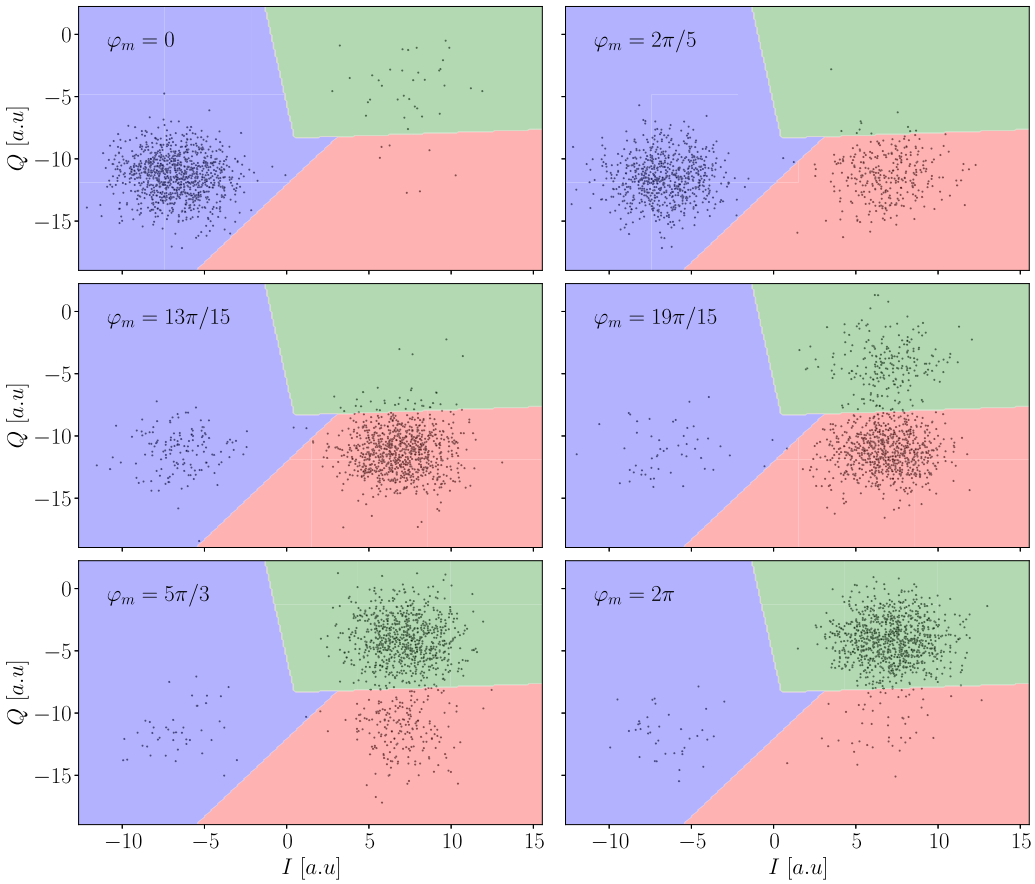

FIG. 9. Example of data distribution associated to the sequential charging protocol. Each plot shows the results (black dots) in the (I, Q) plane (in arbitrary units) as a function of φ_m. For each state shown in the plot, we have considered 1024 runs. These measurements have been carried out using the *ibm_auckland* device. The background is colored according to that discussed in the calibration phase. In particular, the blue part is classified as $|0\rangle$, the red one as $|1\rangle$, and the green one as $|2\rangle$.

(up to a constant) to

$$\omega_n = (\omega_P - E_C)n - \tfrac{1}{2}E_C n(n-1). \tag{A10}$$

From this, we finally derive

$$\Delta = \omega_1 - \omega_0 = \omega_P - E_C, \tag{A11}$$

$$\Delta' = \omega_2 - \omega_1 = \omega_P - 2E_C = \Delta - E_C, \tag{A12}$$

$$\Delta_{\max} = \omega_2 - \omega_0 = \Delta + \Delta' = 2\omega_P - 3E_C. \tag{A13}$$

These parameters are the ones considered in the main text. As a final comment, it is easy to note that $\Delta > \Delta'$, as assumed in our analysis.

APPENDIX B: CALIBRATION AND DATA ANALYSIS

The reconstruction of the state of a transmon, after the application of a time-dependent external drive, is done through a readout in the so-called dispersive regime. Here, a harmonic oscillator (LC circuit playing the role of a resonator) is weakly coupled to the transmon and off resonant with respected to it [40]. In this regime the frequency of the oscillator depends of the state of the transmon. This allows for a so called non-destructive measurement [56] based on the fact that a monochromatic microwave with frequency Ω_0 applied to the resonator is modified in such a way that

$$\cos\Omega_0 t \to A\cos(\Omega_0 t + \chi), \tag{B1}$$

with A and χ real numbers representing an amplitude and a phase, respectively. Taking into account the complex representation of the transmitted wave at a given time, one can write

$$Ae^{i\chi} = I + iQ, \tag{B2}$$

with I and Q real numbers. Every measurement of the transmon state is therefore reported as a point in the (I, Q) plane. To accumulate proper statistics, the machine performs multiple runs (1024 in default settings). They are typically very scattered, requiring further analysis to extract meaningful information from them. We have classified the points according to the three relevant states of the system ($|0\rangle$, $|1\rangle$, and $|2\rangle$) by means of scikit-learn, an open-source machine-learning library based on the Python programming language [57]. We have used support vector machines method with linear kernel function. This method takes as input two arrays: an array X of shape $(n\_samples, n\_features)$ holding the training samples and an array y of class labels, that can be strings or integers, of shape $(n\_samples)$. In our case, we have 3072 samples with two features, I and Q, and three possible labels: 0, 1, or 2. After being trained, the model can be used to classify new values.

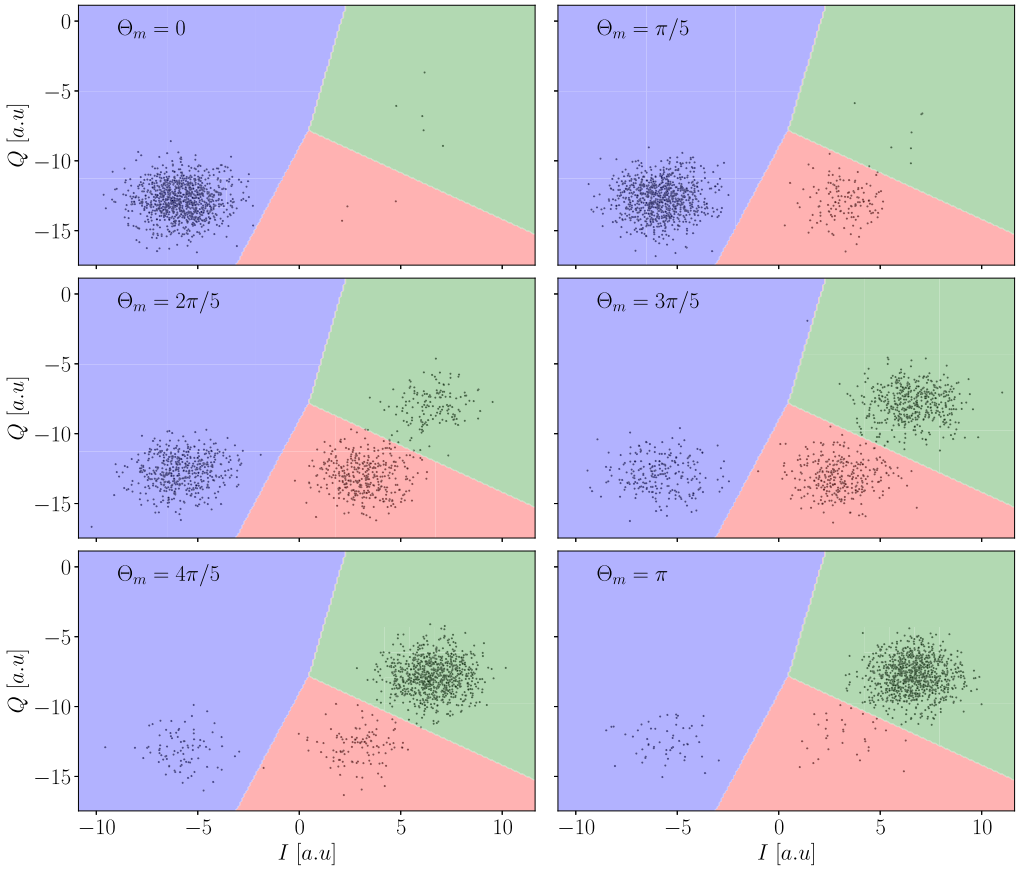

FIG. 10. Example of data distribution associated to the simultaneous charging protocol. Each plot shows the results (black dots) in the (I, Q) plane (in arbitrary units) as a function of Θ_m. For each state shown in the plot, we have considered 1024 runs. These measurements have been carried out using the *ibmq_toronto* device. The background is colored according to that discussed in the calibration phase. In particular, the blue part is classified as $|0\rangle$, the red one as $|1\rangle$, and the green one as $|2\rangle$.

Figure 8 shows an example of data distribution with the colored regions graphically representing the data labels. According to this picture, the energy stored in a qutrit QB (with respect to the ground state) can be determined through the relation

$$E(\eta) = \Delta \mathcal{P}_1(\eta) + \Delta_{\max} \mathcal{P}_2(\eta), \tag{B3}$$

with

$$\mathcal{P}_i(\eta) = |\langle \Psi(\eta) | i \rangle|^2 \tag{B4}$$

and $\eta = \varphi_m, \Theta_m$, depending on the considered charging protocol.

In Figs. 9 and 10, we show the different evolutions of the state of the qutrit in the (I, Q) plane considering the sequential and simultaneous charging, respectively. In particular, while in the former case there is an intermediate situation in which the system is in state $|1\rangle$ with high probability, this doesn't happen in the latter.

APPENDIX C: ADIABATIC CHARGING OF THE THREE-LEVEL QB

An alternative way to charge the qutrit QB realizing a stable $|0\rangle \to |2\rangle$ transition involves a classical charging [see (21)], with two identical time-dependent drives such that

$$f_1(t) = f_2(t) = f(t) \tag{C1}$$

and

$$\Omega_1 = \Omega_2 = \frac{\Delta + \Delta'}{2}, \tag{C2}$$

namely, resonant with a unique frequency given by the average of the two-level spacing [58]. Under such conditions, assuming again the RWA, one obtains the new effective Hamiltonian

$$\hat{\mathcal{H}}^{(3)}_{\text{eff}}(t) = \frac{g}{2} f(t) \begin{pmatrix} 0 & e^{-i\delta t} & 0 \\ e^{i\delta t} & 0 & e^{i\delta t} \\ 0 & e^{-i\delta t} & 0 \end{pmatrix}, \tag{C3}$$

with

$$\delta = \frac{\Delta - \Delta'}{2}. \tag{C4}$$

Note that, according to the derivation reported in Appendix A, this parameter is positive and can be written only in terms of the transmon charging energy, namely,

$$\delta = \frac{E_C}{2}. \tag{C5}$$

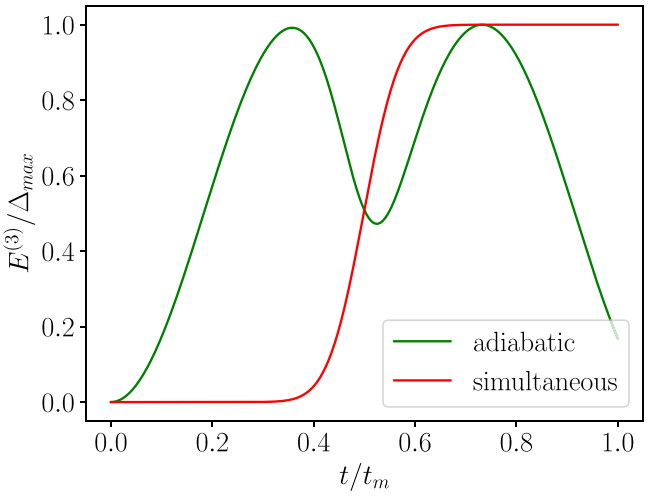

FIG. 11. Energy stored in the qutrit QB (in units of $\Delta_{\max}$) as a function of t (in units of t_m) for both an adiabatic (green curve) and simultaneous (red curve) charging protocol. Here we have considered the same Gaussian pulses as in the qubit case.

To solve the dynamics, in this case it is possible to consider a full numerical approach. However, in the following we will proceed along a different path based on the adiabatic approximation [59], which will allow us to have a better insight of the physics of the system. In this case, the state of the system at a given time t can be approximated as

$$|\Psi'(t)\rangle \approx \sum_{\sigma} c_\sigma e^{-i\int_0^t E_\sigma(\tau)d\tau} e^{i\gamma_\sigma(t)} |\Psi_\sigma(t)\rangle \quad \sigma = B, \pm. \tag{C6}$$

In the above expression, one needs to take into account the instantaneous eigenstates of the Hamiltonian in (C3),

$$|\Psi_B(t)\rangle = \begin{pmatrix} -\frac{1}{\sqrt{2}} \\ 0 \\ \frac{1}{\sqrt{2}} \end{pmatrix}; \quad |\Psi_\pm(t)\rangle = \begin{pmatrix} \frac{1}{2} \\ \pm\frac{e^{i\delta t}}{\sqrt{2}} \\ \frac{1}{2} \end{pmatrix}, \tag{C7}$$

with instantaneous energy eigenvalues

$$E_B(t) = 0, \quad E_\pm(t) = \pm\frac{g}{\sqrt{2}} f(t). \tag{C8}$$

Other important terms which compare to (C6) are the geometric or Berry phases [59]:

$$\gamma_B(t) = i\int_0^t d\tau \langle\Psi_B(t)|\frac{d}{d\tau}|\Psi_B(t)\rangle = 0,$$

$$\gamma_\pm(t) = i\int_0^t d\tau \langle\Psi_\pm(t)|\frac{d}{d\tau}|\Psi_\pm(t)\rangle = -\frac{\delta t}{2}. \tag{C9}$$

Taking into account the initial condition already discussed in the main text, namely,

$$c_B = \frac{1}{\sqrt{2}}; \quad c_\pm = \frac{1}{2}, \tag{C10}$$

one finally obtains

$$|\Psi'(t)\rangle \approx \begin{pmatrix} \frac{1}{2}\left[\cos\Theta(t)e^{-i\frac{\delta t}{2}} - 1\right] \\ -\frac{i}{\sqrt{2}}\sin\Theta(t)e^{i\frac{\delta t}{2}} \\ \frac{1}{2}\left[\cos\Theta(t)e^{-i\frac{\delta t}{2}} + 1\right] \end{pmatrix}, \tag{C11}$$

with stored energy

$$E_{\rm ad}^{(3)}(t) \approx \frac{\Delta}{2}\sin^2\Theta(t) + \frac{\Delta_{\max}}{4}\left[1 - 2\cos\Theta(t)\cos\left(\frac{\delta t}{2}\right) + \cos^2\Theta(t)\right]. \tag{C12}$$

In the regime where both approaches are applicable, the adiabatic charging usually leads to a faster but less stable charging with respect to the simultaneous one (see Fig. 11).

[1] F. Campaioli, F. A. Pollock, and S. Vinjanampathy, Quantum batteries, in *Thermodynamics in the Quantum Regime: Fundamental Aspects and New Directions*, edited by F. Binder, L. A. Correa, C. Gogolin, J. Anders, and G. Adesso (Springer International Publishing, Cham, 2018), pp. 207–225.

[2] S. Bhattacharjee and A. Dutta, Quantum thermal machines and batteries, Eur. Phys. J. B **94**, 239 (2021).

[3] M. Polini, F. Giazotto, K. C. Fong, I. M. Pop, C. Schuck, T. Boccali, G. Signorelli, M. D'Elia, R. H. Hadfield, V. Giovannetti, D. Rossini, A. Tredicucci, D. K. Efetov, F. H. L. Koppens, P. Jarillo-Herrero, A. Grassellino, and D. Pisignano, Materials and devices for fundamental quantum science and quantum technologies, arXiv:2201.09260.

[4] F. Campaioli, S. Gherardini, J. Q. Quach, M. Polini, and G. M. Andolina, Colloquium: Quantum batteries, arXiv:2308.02277.

[5] H. Tajima, N. Shiraishi, and K. Saito, Uncertainty relations in implementation of unitary operations, Phys. Rev. Lett. **121**, 110403 (2018).

[6] H. Tajima, N. Shiraishi, and K. Saito, Coherence cost for violating conservation laws, Phys. Rev. Res. **2**, 043374 (2020).

[7] G. Chiribella, Y. Yang, and R. Renner, Fundamental energy requirement of reversible quantum operations, Phys. Rev. X **11**, 021014 (2021).

[8] R. Alicki and M. Fannes, Entanglement boost for extractable work from ensembles of quantum batteries, Phys. Rev. E **87**, 042123 (2013).

[9] F. C. Binder, S. Vinjanampathy, K. Modi, and J. Goold, Quantacell: powerful charging of quantum batteries, New J. Phys. **17**, 075015 (2015).

[10] G. M. Andolina, D. Farina, A. Mari, V. Pellegrini, V. Giovannetti, and M. Polini, Charger-mediated energy transfer in exactly solvable models for quantum batteries, Phys. Rev. B **98**, 205423 (2018).

[11] A. Crescente, D. Ferraro, M. Carrega, and M. Sassetti, Enhancing coherent energy transfer between quantum devices via a mediator, Phys. Rev. Res. **4**, 033216 (2022).

[12] X. Yang, Y.-H. Yang, M. Alimuddin, R. Salvia, S.-M. Fei, L.-M. Zhao, S. Nimmrichter, and M.-X. Luo, Battery capacity of energy-storing quantum systems, Phys. Rev. Lett. **131**, 030402 (2023).

[13] A. Crescente, D. Ferraro, and M. Sassetti, Boosting energy transfer between quantum devices through spectrum engineering in the dissipative ultrastrong coupling regime), arXiv:2312.12034.
[14] F. Campaioli, F. A. Pollock, F. C. Binder, L. Céleri, J. Goold, S. Vinjanampathy, and K. Modi, Enhancing the charging power of quantum batteries, Phys. Rev. Lett. **118**, 150601 (2017).
[15] T. P. Le, J. Levinsen, K. Modi, M. M. Parish, and F. A. Pollock, Spin-chain model of a many-body quantum battery, Phys. Rev. A **97**, 022106 (2018).
[16] D. Rossini, G. M. Andolina, D. Rosa, M. Carrega, and M. Polini, Quantum advantage in the charging process of Sachdev-Ye-Kitaev batteries, Phys. Rev. Lett. **125**, 236402 (2020).
[17] D. Rosa, D. Rossini, G. M. Andolina, M. Polini, and M. Carrega, Ultra-stable charging of fast-scrambling SYK quantum batteries, J. High Energy Phys. 11 (2020) 067.
[18] J. Q. Quach and W. J. Munro, Using dark states to charge and stabilize open quantum batteries, Phys. Rev. Appl. **14**, 024092 (2020).
[19] J.-Y. Gyhm, D. Šafránek, and D. Rosa, Quantum charging advantage cannot be extensive without global operations, Phys. Rev. Lett. **128**, 140501 (2022).
[20] D. Ferraro, M. Campisi, G. M. Andolina, V. Pellegrini, and M. Polini, High-power collective charging of a solid-state quantum battery, Phys. Rev. Lett. **120**, 117702 (2018).
[21] A. Crescente, M. Carrega, M. Sassetti, and D. Ferraro, Ultrafast charging in a two-photon Dicke quantum battery, Phys. Rev. B **102**, 245407 (2020).
[22] A. Delmonte, A. Crescente, M. Carrega, D. Ferraro, and M. Sassetti, Characterization of a two-photon quantum battery: Initial conditions, stability and work extraction, Entropy **23**, 612 (2021).
[23] F.-Q. Dou, Y.-Q. Lu, Y.-J. Wang, and J.-A. Sun, Extended Dicke quantum battery with interatomic interactions and driving field, Phys. Rev. B **105**, 115405 (2022).
[24] S. Seah, M. Perarnau-Llobet, G. Haack, N. Brunner, and S. Nimmrichter, Quantum speed-up in collisional battery charging, Phys. Rev. Lett. **127**, 100601 (2021).
[25] V. Shaghaghi, V. Singh, G. Benenti, and D. Rosa, Micromasers as quantum batteries, Quantum Sci. Technol. **7**, 04LT01 (2022).
[26] F. Zhao, F.-Q. Dou, and Q. Zhao, Charging performance of the Su-Schrieffer-Heeger quantum battery, Phys. Rev. Res. **4**, 013172 (2022).
[27] P. A. Erdman, G. M. Andolina, V. Giovannetti, and F. Noé, Reinforcement learning optimization of the charging of a Dicke quantum battery, arXiv:2212.12397.
[28] V. Shaghaghi, V. Singh, M. Carrega, D. Rosa, and G. Benenti, Lossy micromaser battery: Almost pure states in the Jaynes-Cummings regime, Entropy **25**, 430 (2023).
[29] G. Gemme, G. M. Andolina, F. M. D. Pellegrino, M. Sassetti, and D. Ferraro, Off-resonant Dicke quantum battery: Charging by virtual photons, Batteries **9**, 197 (2023).
[30] C. Rodríguez, D. Rosa, and J. Olle, Artificial intelligence discovery of a charging protocol in a micromaser quantum battery, Phys. Rev. A **108**, 042618 (2023).
[31] F.-Q. Dou and F.-M. Yang, Superconducting transmon qubit-resonator quantum battery, Phys. Rev. A **107**, 023725 (2023).
[32] J. Q. Quach, K. E. McGhee, L. Ganzer, D. M. Rouse, B. W. Lovett, E. M. Gauger, J. Keeling, G. Cerullo, D. G. Lidzey, and T. Virgili, Superabsorption in an organic microcavity: Toward a quantum battery, Sci. Adv. **8**, eabk3160 (2022).
[33] Y.-Y. Zhang, T.-R. Yang, L. Fu, and X. Wang, Powerful harmonic charging in a quantum battery, Phys. Rev. E **99**, 052106 (2019).
[34] A. Crescente, M. Carrega, M. Sassetti, and D. Ferraro, Charging and energy fluctuations of a driven quantum battery, New J. Phys. **22**, 063057 (2020).
[35] F. Mazzoncini, V. Cavina, G. M. Andolina, P. A. Erdman, and V. Giovannetti, Optimal control methods for quantum batteries, Phys. Rev. A **107**, 032218 (2023).
[36] C.-K. Hu, J. Qiu, P. J. P. Souza, J. Yuan, Y. Zhou, L. Zhang, J. Chu, X. Pan, L. Hu, J. Li, Y. Xu, Y. Zhong, S. Liu, F. Yan, D. Tan, R. Bachelard, C. J. Villas-Boas, A. C. Santos, and D. Yu, Optimal charging of a superconducting quantum battery, Quantum Sci. Technol. **7**, 045018 (2022).
[37] A. C. Santos, B. Çakmak, S. Campbell, and N. T. Zinner, Stable adiabatic quantum batteries, Phys. Rev. E **100**, 032107 (2019).
[38] G. Gemme, M. Grossi, D. Ferraro, S. Vallecorsa, and M. Sassetti, Ibm quantum platforms: A quantum battery perspective, Batteries **8**, 43 (2022).
[39] J. Koch, T. M. Yu, J. Gambetta, A. A. Houck, D. I. Schuster, J. Majer, A. Blais, M. H. Devoret, S. M. Girvin, and R. J. Schoelkopf, Charge-insensitive qubit design derived from the Cooper pair box, Phys. Rev. A **76**, 042319 (2007).
[40] P. Krantz, M. Kjaergaard, F. Yan, T. P. Orlando, S. Gustavsson, and W. D. Oliver, A quantum engineer's guide to superconducting qubits, Appl. Phys. Rev. **6**, 021318 (2019).
[41] T. Alexander, N. Kanazawa, D. J. Egger, L. Capelluto, C. J. Wood, A. Javadi-Abhari, and D. C. McKay, Qiskit pulse: Programming quantum computers through the cloud with pulses, Quantum Sci. Technol. **5**, 044006 (2020).
[42] K. N. Smith, G. S. Ravi, T. Alexander, N. T. Bronn, A. R. R. Carvalho, A. Cervera-Lierta, F. T. Chong, J. M. Chow, M. Cubeddu, A. Hashim, L. Jiang, O. Lanes, M. J. Otten, D. I. Schuster, P. Gokhale, N. Earnest, and A. Galda, Programming physical quantum systems with pulse-level control, Front. Phys. **10**, 900099 (2022).
[43] S. Schweber, On the application of Bargmann Hilbert spaces to dynamical problems, Ann. Phys. **41**, 205 (1967).
[44] R. Graham and M. Höhnerbach, Two-state system coupled to a boson mode: Quantum dynamics and classical approximations, Z. Phys. B **57**, 233 (1984).
[45] W. Schleich, *Quantum Optics in Phase Space* (John Wiley & Sons, Weinheim, 2011).
[46] Z. Lü and H. Zheng, Effects of counter-rotating interaction on driven tunneling dynamics: Coherent destruction of tunneling and Bloch-Siegert shift, Phys. Rev. A **86**, 023831 (2012).
[47] M. Carrega, A. Crescente, D. Ferraro, and M. Sassetti, Dissipative dynamics of an open quantum battery, New J. Phys. **22**, 083085 (2020).
[48] IBM Quantum, https://quantum-computing.ibm.com (2021).
[49] A. Cervera-Lierta, M. Krenn, A. Aspuru-Guzik, and A. Galda, Experimental high-dimensional Greenberger-Horne-Zeilinger entanglement with superconducting transmon qutrits, Phys. Rev. Appl. **17**, 024062 (2022).
[50] A. Crescente, D. Ferraro, M. Carrega, and M. Sassetti, Analytically solvable model for qubit-mediated energy transfer between quantum batteries, Entropy **25**, 758 (2023).
[51] This device was officially retired by IBM on November 9, 2023.

[52] This device was officially retired by IBM on April 10, 2023.

[53] IBM assistance office (private communication).

[54] D. Jankovi, J.-G. Hartmann, M. Ruben, and P.-A. Hervieux, Noisy qudit vs multiple qubits: Conditions on gate efficiency, arXiv:2302.04543.

[55] H. C. Nguyen, B. G. Bach, T. D. Nguyen, D. M. Tran, D. V. Nguyen, and H. Q. Nguyen, Simulating neutrino oscillations on a superconducting qutrit, Phys. Rev. D **108**, 023013 (2023).

[56] E. Jeffrey, D. Sank, J. Y. Mutus, T. C. White, J. Kelly, R. Barends, Y. Chen, Z. Chen, B. Chiaro, A. Dunsworth, A. Megrant, P. J. J. O'Malley, C. Neill, P. Roushan, A. Vainsencher, J. Wenner, A. N. Cleland, and J. M. Martinis, Fast accurate state measurement with superconducting qubits, Phys. Rev. Lett. **112**, 190504 (2014).

[57] F. Pedregosa, G. Varoquaux, A. Gramfort, V. Michel, B. Thirion, O. Grisel, M. Blondel, P. Prettenhofer, R. Weiss, V. Dubourg *et al.*, scikit-learn: Machine learning in Python, J. Mach. Learn. Res. **12**, 2825 (2011).

[58] D. Willsch, D. Rieger, P. Winkel, M. Willsch, C. Dickel, J. Krause, Y. Ando, R. Lescanne, Z. Leghtas, N. T. Bronn, P. Deb, O. Lanes, Z. K. Minev, B. Dennig, S. Geisert, S. Günzler, S. Ihssen, P. Paluch, T. Reisinger, R. Hanna *et al.*, Observation of Josephson harmonics in tunnel junctions, Nat. Phys. (2024), doi:10.1038/s41567-024-02400-8.

[59] M. V. Berry, Quantal phase factors accompanying adiabatic changes, Proc. R. Soc. London A **392**, 45 (1984).